

Article

Assessment of Data Capture Conditions Effect on Reverse Electrodialysis Process Using a DC Electronic Load

Jesus Nahum Hernandez-Perez ^{1,2}, Marco Antonio Hernández-Nochebuena ³, Jéssica González-Scott ¹, Rosa de Guadalupe González-Huerta ¹, José Luis Reyes-Rodríguez ¹ and Alfredo Ortiz ^{2,*}

¹ Instituto Politécnico Nacional—ESIQIE, Laboratorio de Electroquímica, UPALM, Mexico City 07738, Mexico; jesus-nahum.hernandez@alumnos.unican.es (J.N.H.-P.); jgonzalezs1704@alumno.ipn.mx (J.G.-S.); rgonzalez@ipn.mx (R.d.G.G.-H.); jlreyes@ipn.mx (J.L.R.-R.)

² Department of Chemical and Biomolecular Engineering, Universidad de Cantabria, Av. Los Castros 46, 39005 Santander, Spain

³ Instituto Mexicano del Transporte, Pedro Escobedo 76703, Mexico; marco.hernandez@imt.mx

* Correspondence: alfredo.ortizsainz@unican.es; Tel.: +34-942-200-870

Abstract: Reverse electrodialysis (RED), an emerging membrane-based technology, harnesses salinity gradient energy for sustainable power generation. Accurate characterization of electrical parameters in RED stacks is crucial to monitoring its performance and exploring possible applications. In this study, a DC electronic load module (DCELM) is implemented in a constant current condition (CC mode) for characterization of lab scale RED process, using a RED prototype in-house designed and manufactured (RU1), at different data capture setups (DCS), on which the total number of steps for data capture (NS) and the number of measurements per step (ρ) are the parameters that were modified to study their effect on obtained electrical parameters in RED. NS of 10, 50, and 100 and ρ of 10 and 20 were used with this purpose. The accuracy of resulting current and voltage steps can be enhanced by increasing NS and ρ values, and according to obtained results, the higher accuracy of resulting output current and voltage steps, with low uncertainty of the average output steps (AOS) inside the operational region of power curve, was obtained using a DCS of $NS = 100$ and $\rho = 20$. The developed DCELM is a low-cost alternative to commercial electronic load devices, and the proposed methodology in this study represents an adaptative and optimizable CC mode characterization of RED process. The results obtained in this study suggest that data capture conditions have a direct influence of RED performance, and the accuracy of electrical parameters can be improved by optimizing the DCS parameters, according to the required specifications and the scale of RED prototypes.

Keywords: salinity gradient energy; reverse electrodialysis; red characterization; power production



Citation: Hernandez-Perez, J.N.; Hernández-Nochebuena, M.A.; González-Scott, J.; González-Huerta, R.d.G.; Reyes-Rodríguez, J.L.; Ortiz, A. Assessment of Data Capture Conditions Effect on Reverse Electrodialysis Process Using a DC Electronic Load. *Energies* **2023**, *16*, 7282. <https://doi.org/10.3390/en16217282>

Academic Editor: Svetlozar G. Velizarov

Received: 10 October 2023
Revised: 20 October 2023
Accepted: 23 October 2023
Published: 26 October 2023



Copyright: © 2023 by the authors. Licensee MDPI, Basel, Switzerland. This article is an open access article distributed under the terms and conditions of the Creative Commons Attribution (CC BY) license (<https://creativecommons.org/licenses/by/4.0/>).

1. Introduction

Humanity is currently searching for alternative energy sources to fossil fuels, to reduce CO₂ emissions and other greenhouse gases that are producing the climate change phenomenon [1,2]. Among several renewable energies sources, salinity gradient energy (SGE) is widely spread along littorals and coasts all over the world, wherever a freshwater stream is discharged into the ocean. The amount of thermodynamic energy released from the mixing process (ΔG_{mix}) is proportional to the concentration gradient and the chemical potential difference between the initial state and the mixed state of the solutions [3,4]. SGE has remarkable advantages regarding other renewable energies, some of which are related to its availability in both diurnal and nocturnal periods over the year if the employed feed waters become from natural sources [5,6], the possibility of regulate the amount of power generated with process parameters without CO₂ emissions and the fact that it can be obtained from residual streams of other process, such as reverse osmosis brines or municipal waste water treatment plants [7,8]. However, only a fraction of theoretical

potential of rivers and oceans can be recovered in a practical form, which is known as world technical potential and its value is around 0.2–1 TW, according to the employed technique for energy harvest and the concentration of feed solutions [3,9].

Reverse electro dialysis (RED) is an emerging technology that allows converting some part of the ΔG_{mix} of two water streams (with a different salt concentration) into electricity, through an ion exchange membranes (IEM) stack and redox reactions. Figure 1 shows a schematic representation of a RED unit, which is composed of a membrane stack and the electrode system [10–12].

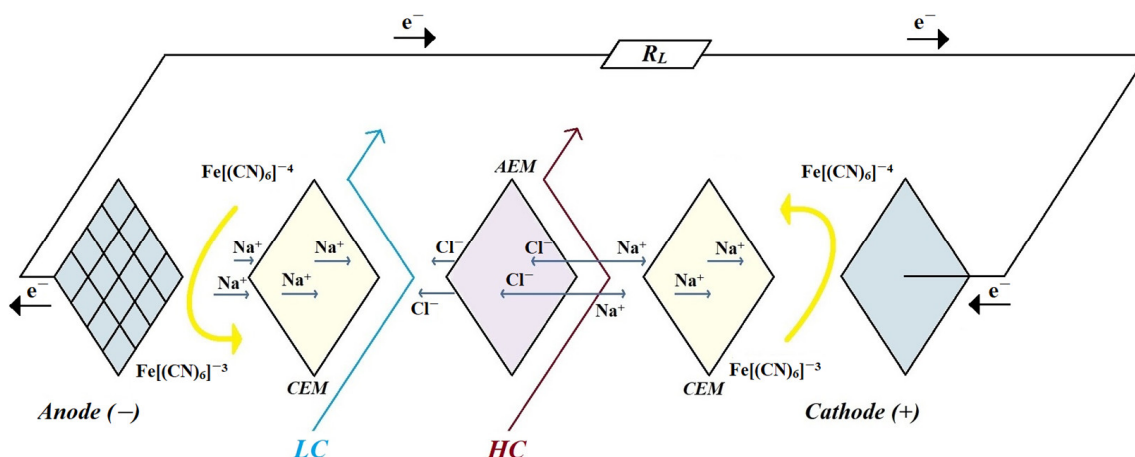


Figure 1. Schematic diagram of a RED unit.

In RED, the cation exchange membrane (CEM) and the anion exchange membrane (AEM) are stacked alternately between two electrodes (anode and cathode), and the intermembrane space is flooded with high concentration (HC) and low concentration (LC) solutions, which flow in sequence one after the other. By this, a membrane cell pair (or simply just a cell) is formed.

A RED stack normally uses a large number of cells (around dozens to hundreds) [5,11] and when an external load (R_L) is connected to the RED unit, the electrode system transforms the available electromotive force into electricity, using charge transfer process on the electrodes surfaces [11,13–15]. As soon as ions move through the membrane stack, they encounter the electrode rinse solution (ERS) at the electrode compartment, which is recirculated across the end plates of the RED unit and is normally composed of a highly reversible redox pair [16,17]. As a result, electrons can be transferred from the anode to the cathode across the equivalent circuit formed (a representation of equivalent circuit is provided in Figure S1).

RED Process Parameters and Characterization

To obtain RED process performance curves, several R_L values must be used to determine the maximum power output that the system can generate to cover an electrical service or application. The Nernst equation can be used to obtain the theoretical electromotive force per cell (E_{Cell}) and of the whole stack (OCV_{Theo}) [3,5,10,18]. Equation (A1) of Appendix A shows the Nernst equation and its parameters.

The amount of energy that can be obtained from a RED unit is determined by the output voltage (which is the actual potential that the RED device delivers to R_L), at a determined current demand condition, and the internal resistance (R_i) of the RED unit. In principle, R_i is composed of the ohmic and non-ohmic components on the membrane stack resistance (R_{Stack}) and the electrode system resistance (R_{Elec}) [5,11,13]. Normally R_{Stack} represents the main contribution to R_i , while R_{Elec} is not critical if the proper electrode material is selected and if the stack is composed of several cells [5,17]. Equations (A3) and (A4) of Appendix A describe the R_i components.

In RED, several variables have a direct influence on OCV_{Theo} , R_i , and (consequently) the obtained power density (P_d). The input parameters can be classified into those that depend on “feed parameters” and those that depend on “RED unit parameters” [5,11,18,19]. Figure 2a shows a schematic representation of the RED process parameters classification.

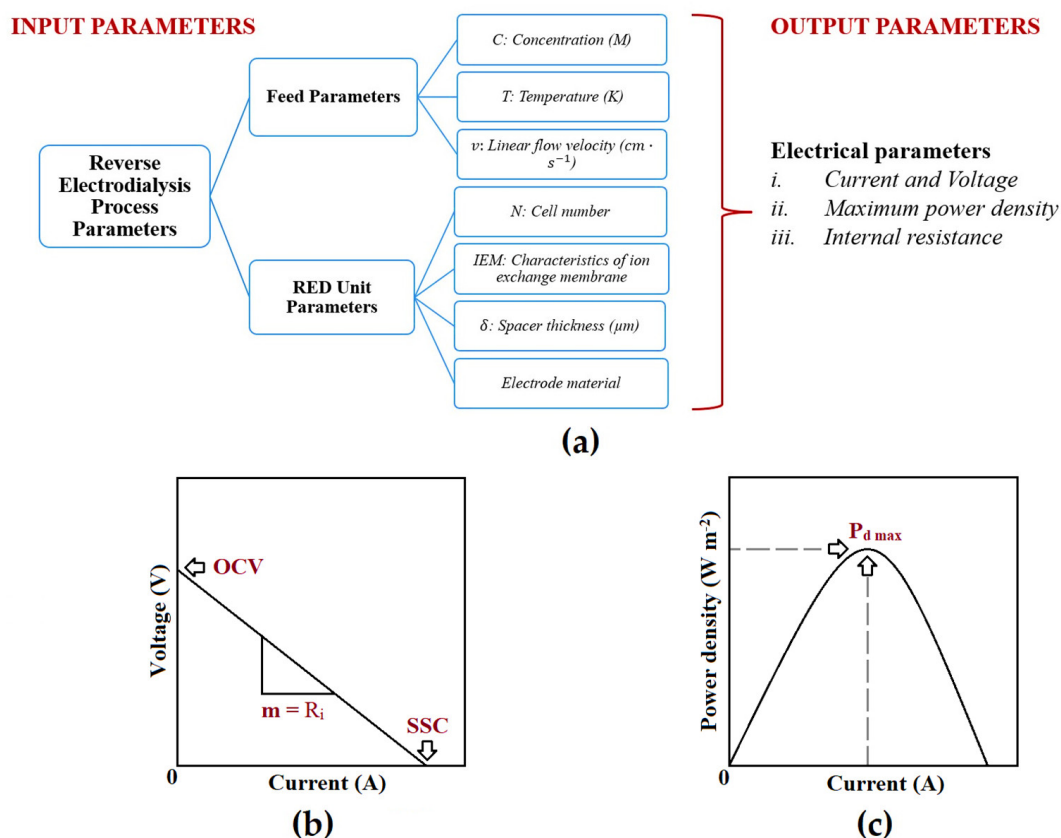


Figure 2. (a) Considered parameters in reverse electro dialysis process; (b) voltage vs. current relationship (polarization curve) and (c) power density vs. current relationship (power curve) obtained in a typical RED process.

The feed parameters describe the properties of feed solutions (concentration, temperature, and flow regime), while RED unit parameters are referred to the characteristics of the RED stack and the electrode system (cell number (N), properties of IEM used to conform the stack (ion exchange capacity, permselectivity, intrinsic resistance, etc.), the intermembrane space (δ), and the electrode material) [5,11,18]. The linear flow velocity (v) can be defined as the fluid velocity inside one flow compartment formed by the spacer and is related to the residence time and hydrodynamic behavior of the feed solutions. Based on the stack dimensions, this parameter can be obtained for determined volumetric flow conditions [11]. Equations (A12) and (A13) of Appendix A describes how to calculate v . The proper selection of the electrode material assures that the electron transfer process at the surface will be reversible at the lowest overpotential possible [13,17]. Although the membrane properties are normally considered as the limiting parameters of a RED unit, the rest of the components also have a relevant effect on E_{Stack} and R_i on a different level. In the case of a RED operation, the apparent permselectivity ($\bar{\alpha}$) can be considered for both CEM and AEM as an average parameter that describes in a general form the ability of the membranes to allow the pass to counter-ions and inhibit it for co-ions [5,20], as can be seen in Equation (A14) of Appendix A.

The output parameters can be referred to as electrical parameters. They describe the current–voltage response generated by the RED unit at different R_L conditions. The slope of the output voltage (U) vs. output current (I) relationship (also called the polarization curve)

represents an approximation of R_i , as can be seen in Figure 2b. The open circuit voltage (OCV) condition occurs when the R_L value is very high concerning R_i , so electrons cannot be transferred from the anode to the cathode across the circuit. The short circuit current (SCC) is a condition where R_L is close to zero, so I have a maximum intensity value while U drops close to zero. The P_d can be defined as the product of current times voltage, divided by the membrane active area (as is described in Equations (A10) and (A11) of Appendix A), and can be represented as a power curve (Figure 2c) by plotting P_d vs. I . Thus, the top of the curve represents the maximum power density ($P_{d\ max}$) that can be generated under a determined input parameters condition.

To determine the electrical parameters of RED devices several methods are reported in the literature. Table 1 describes some examples of the mentioned characterization methods for RED devices reported in the literature. In all these methods, the purpose is to determine polarization curves, which can be used to obtain R_i and experimental open circuit voltage (OCV_{Stack}), power curves which can be used to define the operation zone of the RED unit, and the maximum power density ($P_{d\ max}$) that can be produce.

Table 1. Characterization methods for RED process reported in the literature.

Instruments Employed for RED Characterization	Data Capture Conditions	Ref.
Rheostat Voltage: Multimeter UNI-T (UT71D)) Current: Fluke 45 Dual Display Multimeter	<ul style="list-style-type: none"> OCV condition: 5 min Time for stabilization until data capture: 120 s 	[21]
Rheostat Voltage and Current: Multimeter Amprobe AM-520	<ul style="list-style-type: none"> Resistance Range: 0.5–100 Ω 	[22]
Rheostat Voltage: Datalogger (LabVIEW™, National Instruments) Current: external Amperemeter	<ul style="list-style-type: none"> Resistance Range: 0–22 Ω OCV condition: ~5 min 1 h of operation from OCV until OCV/2 Data capture at a frequency of 1 Hz 	[23]
Rheostat: Five-decade resistance box (COPRICO) Voltage: 3 1/2 Digital multimeter (Veleman, DVM760) Current: 6 1/2 Digital multimeter (Agilent, 34422A)	<ul style="list-style-type: none"> OCV, R_i and P_d max were determined by means of linear regression and parabolic correlation 	[24]
Potentiostat/Galvanostat (HAB-151). Recorded data were processed using a data logging system (midi LOGGER GL200, GRAPHTEC Co.)	<ul style="list-style-type: none"> Current range: From OCV until SCC Scan rate: 0.4 mA s⁻¹ 	[25]
Potentiostat/Galvanostat (Ivium Technologies) in the galvanostatic mode	<ul style="list-style-type: none"> Current range: From OCV until SCC Scan rate: 2 mA s⁻¹ 	[26]
Potentiostat/Galvanostat Metrohm Autolab PGSTAT302N equipped with an FRA module	<ul style="list-style-type: none"> Current range: 0–40 A m⁻² Current steps: 17 Time per step: 40 s 	[27]
Potentiostat/Galvanostat (Ivium Technologies) using a chronopotentiometric method	<ul style="list-style-type: none"> Current range: 0–40 A m⁻² Current steps: 20 Time per step: 30 s 	[28]
Electronic load in CC mode (Chroma Systems Solutions 63103A)	<ul style="list-style-type: none"> OCV condition: ~5 min Current rate: 0.025 A Values were obtained until the system reach a steady-state 	[10]
Electronic load in CC mode (Chroma Systems Solutions 63103A)	<ul style="list-style-type: none"> Current range: 0–1 A Values were obtained until the system reach a steady-state 	[29]

Table 1. Cont.

Instruments Employed for RED Characterization	Data Capture Conditions	Ref.
Electronic load in CC mode (Chroma Systems Solutions 63103A)	<ul style="list-style-type: none"> • Values were obtained until the system reach a steady-state 	[8]
Electronic load in CC mode (Chroma Systems Solutions 63103A)	<ul style="list-style-type: none"> • OCV condition: ~5 min • Current rate: 0.025 A • Values were obtained until the system reach a steady-state 	[19]
Electronic load (PLZ 164 W, Kikusui electronics corp.) in I-V mode and CC mode	<ul style="list-style-type: none"> • Current range: From OCV until SCC • I-V mode, Scan rate: 8.1 mA s⁻¹ • CC mode, Current steps: 7, Time per step: 40 min 	[7]

In some works, a rheostat with fixed electrical resistance values is connected to the RED unit for a defined time condition, and the corresponding values of output voltage and current are recorded using an external voltmeter and amperemeter or by using a data logger for data capture [21–24]. Although this method is the simplest and cheapest way for RED characterization, there is no way to control or limit the voltage or the current that the load consumes. The resolution of the resulting polarization and power curves depends on the number of resistances used as well as if their values are suitable to the power supply capacity of the RED unit, which depends on its internal resistance. In other words, if the RED input parameters changes, the selected external resistance values may not be suitable for the new experimental conditions, so adapting to changes in test requirements with fixed resistors is a time-consuming task that requires many resistors. Avci et al. [24] used several fixed resistances for RED characterization, employing a linear regression method to determine OCV_{Stack} as also R_i . However, since the selected resistance values, only a small portion of the power curve was experimentally determined, and a quadratic correlation was used to estimate the entire power curve and the corresponding $P_{d max}$ value. Although this method represents a valid approximation, $P_{d max}$ obtained does not represent a precise experimental value because of the limited experimental points used to obtain the quadratic correlation, which was a consequence of the selected resistance values for characterization.

Other authors have reported the use of potentiostat/galvanostat to perform a current scan from OCV condition to SCC condition at a defined scan rate, measuring the corresponding voltage values [25,26]. Moreover, potentiostat/galvanostat has been employed using chronopotentiometric methods defining a current demand range, divided in several steps at a specific time per step, and by this evaluate the output voltage at every current demand step [27,28]. The use of potentiostat/galvanostat is a more precise method to obtain a high resolution polarization and power curves, since the whole current–voltage relationship from OCV until SCC conditions can be obtained, at the same data capture conditions on every test. Still, the cost of these devices is considerably higher than fixed resistances method since there are normally used to perform several electrochemical tests besides power supply devices characterization.

Lastly, in other studies, a similar technique has been carried out by using an DC electronic load, where a current demand condition can also be defined. A DC electronic load is a programable test instrument designed to characterize DC power supplies by emulating multiple load profiles, offering high flexibility to adapting to changes on experimental conditions. Normally, these devices have several modes of operation, were the most common are constant current condition (CC mode), constant voltage condition (CV mode), constant resistance condition (CR mode), and constant power condition (CP mode) [30]. In case of RED characterization, the most relevant modes reported in the literature are CC mode, where a current demand is established and keep it constant until a new value is

requested, and also changing current condition (I–V mode), where the demanded current is gradually increased at a defined scan rate [7,8,10,19,29].

While potentiostat/galvanostat and DC electronic load devices can be programmed to set data capture conditions on every experiment, the fixed resistances method requires an appropriate data capture software, which is not always reported in the literature and normally this task is performed manually by the operator using a digital multimeter, increasing the uncertainty related to human random errors in the results.

Focusing on characterization using a DC electronic load, while I–V mode is normally used for lab scale characterization of the RED process, where several process parameters are usually compared without considering an equilibrium condition, CC mode results represents a behave of a steady state regime in a long-term operation, which has its relevance for bench scale and pilot plant scale tests [7]. Nevertheless, as can be seen from Table 1, until now there is no direct or undirect consensus on employed method used for RED process characterization, which can lead to a degree of uncertainty in the comparison of results between different groups, despite the use of same input parameters.

In this study, the influence of data capture conditions on a lab scale RED process were analyzed by means of a DC electronic load module (DCELM), which works as an actuator/data capture system, allowing to the reducing of human random error on data capture compared to conventional fixed electrical resistance methods, as also representing a low-cost alternative to commercial potentiation/galvanostat and electronic load devices. The system was developed on an Arduino platform, controlled by an interface in MATLAB® (Ver. R2022b) and operated in the CC mode. The total number of steps for data capture (NS) and the number of measurements per step (ρ) are the data capture setup (DCS) parameters that were modified to compare their influence on accuracy and uncertainty of the determined electrical parameters in RED. The described method in this study represents a quick and reliable tool for RED process analysis, which can used on lab scale conditions, as well as be optimized and adapted to steady state experiments.

2. Materials and Methods

2.1. Reverse Electrodialysis Unit Design (RU1)

A RED unit was designed and built, based on schematics and diagrams available in the literature [20,31], using Nylamid M as base material to conform the end plates of the prototype. A picture of the developed RED prototype (RU1) is presented in Figure S2. Figure S2a correspond to the manufactured endplates while Figure S2b correspond to an image of the prototype before assembly. The stack was composed of five cells and the RED unit parameters used for the experiments are summarized in Table 2.

Table 2. Considered RED unit parameters.

RED Unit Parameters	RU1
Effective area per cell	0.0049 m ²
Effective area of the stack	0.0245 m ²
Cell number (N)	5
Intermembrane distance (δ)	255 μ m
CEM (outer membrane)	Nafion® 324 (Dupont, Wilmington, DE, USA)
CEM (stack)	Fuji Type 10 CEM (Fujifilm, Tilburg, The Netherlands)
AEM (stack)	Fuji Type 10 AEM (Fujifilm)
Electrode material	Pt/Ti mesh electrode
Torque applied	2.5 N·m

The effective area per cell was 0.0049 m². The intermembrane distance was defined by a silicon gasket with a PES mesh-type spacer of the same thickness ($\delta = 255 \mu$ m). As for IEM, Fuji Type 10 membrane (Fujifilm Manufacturing Europe BV, the Netherlands) was used as CEM and AEM in the stack, while Nafion®324 (Dupont, Wilmington, DE, USA) was used as an outer CEM to reduce the permeation of the electrode rinse solution (ERS) from the

electrode compartment to the stack, according to Scialdone et al. [16]. The properties of the employed IEM in the stack are reported in Table S1.

The ERS was composed of 0.05 M $K_4[Fe(CN)_6]$, 0.05 M $K_3[Fe(CN)_6]$ (Aldrich, purity > 99%) and 0.25 M NaCl (Fermont, Mexico City, Mexico. Composition > 99.5%) as supporting electrolyte in deionized water (Fermont, Mexico. Specific Conductance: $1.8 \times 10^{-6} \Omega^{-1} \text{ cm}^{-1}$). A pH of 7.22 was determined for the ERS using a pHmeter PC45 (Conductronic, Puebla, Mexico). Titanium mesh with platinum coating (Pt/Ti mesh) was employed as working electrode material. The electrodes were prepared by sticking Pt/Ti mesh (Fuellcellstore, College Station, TX, USA) and an $\frac{1}{4}$ inch Ti bar (used as a connector) with a conductive epoxy resin SG-3100 S (MG Chemicals, Burlington, ON, Canada). Once the resin was applied, the electrodes were heated until 65 °C for 3 h in an oven (Memert, Schwabach, Germany), and they were cooled at room temperature. Next, they were covered by a nonconductive epoxy resin to capsule the conductive epoxy resin area. This has the purpose of isolating and protecting the joint from corrosion. Figure S3 shows a picture of in-house built electrodes before their use. The electrodes were assembled to the end plates and sealed with an acrylonitrile–butadiene–styrene (ABS) solution (ABS saturated in ketone) and left to dry for 24 h.

2.2. DC Electronic Load Module for RED Applications

A DC electronic load module (DCELM) was designed and integrated for RED applications (a picture of the DCELM is provided in Figure S4). The DCELM is a current demand emulator device and data acquisition system designed to characterize reverse electro dialysis prototypes and power generation systems up to 0.5 Amperes. It is composed of three parts: a communication module, a data acquisition and signal conditioning module and a power module. Together, these components allow the generation of a voltage signal that activates the power circuit, which imposes a load to an external power supply to determine the voltage and current generated. The communication module allows communication between the DCELM and the user through an interface developed in MATLAB® for its control and data capture, as represented in Figure 3.

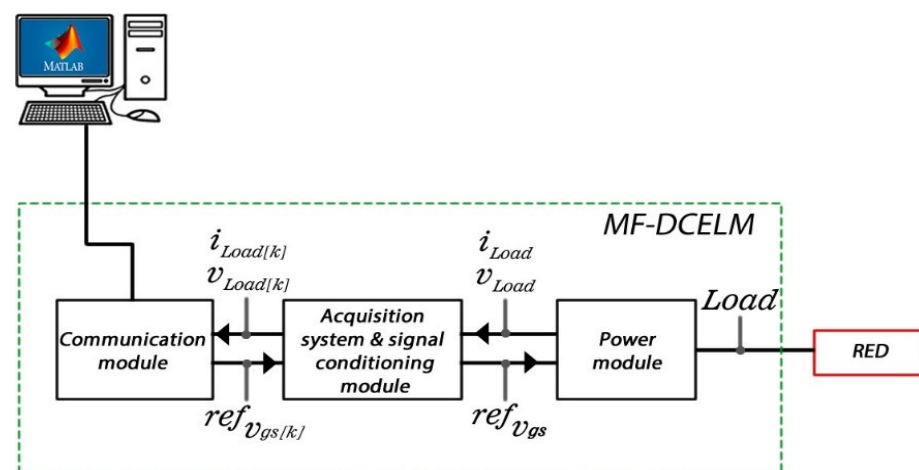


Figure 3. Schematic diagram of DCELM.

The power module is based on a directly polarized N-channel metal-oxide-semiconductor field-effect transistor (MOSFET), configured to operate on its Ohmic region and by this obtain i_{load} and V_{load} (which represent the output current and voltage values of the power generation device). The MOSFET has three terminals: source (*s*), drain (*d*), and gate (*g*). The *g* terminal controls the transistor activation, the *d* terminal is connected to the positive terminal of the power supply device, and the *s* terminal is connected in serial to a current sensor conformed by a shut—resistance of 0.01 Ω , connected with the negative terminal of the power supply device. This is represented in Figure 4a.

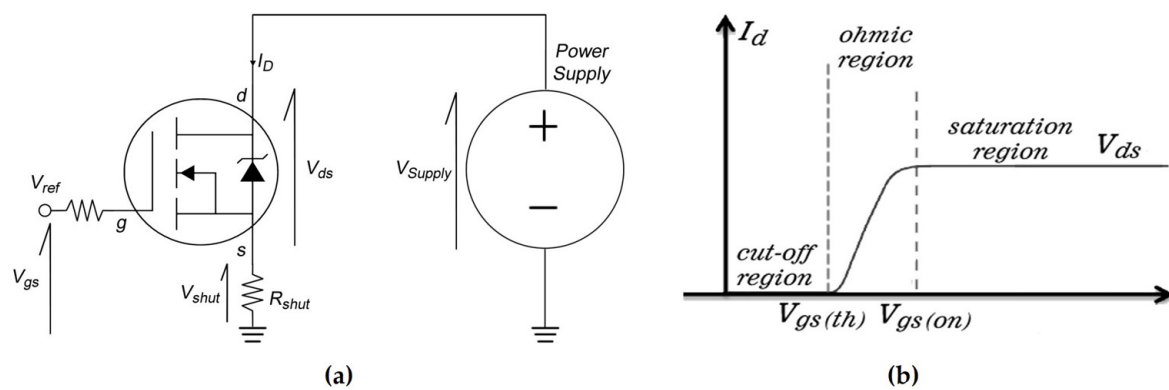


Figure 4. (a) Schematic diagram of the directly polarized circuit in the MOSFET and (b) operational regions and the current demand response of the MOSFET according to the voltage supply V_{gs} .

In general terms, the MOSFET has three operational modes, as it is described in Figure 4b.

Cut region: In this mode there is no current continuity, and the voltage difference between d and s terminals (V_{ds}) has a maximum value (OCV condition) and the voltage difference between g and s terminals (V_{gs}) is minor or equal to zero.

Ohmic region: In this region the MOSFET works as a nonlinear variable resistance whose value is a function of the V_{gs} applied, allowing electrons to flow through the transistor and, by this, obtaining a theoretical drain current (I_D). This region is physically delimited by a threshold voltage in the g terminal ($V_{gs(th)}$), which is the minimum voltage necessary for the electron flow to occur, and the saturation voltage in the g terminal ($V_{gs(on)}$). As the I_D increases, the resistance of the transistor decreases as well as the voltage V_{ds} . On the contrary, if I_D decreases, the internal resistance of the transistor rises, increasing the voltage V_{ds} at the transistor terminals.

Saturation region: At this condition $V_{gs} > V_{gs(on)}$, so the MOSFET overpasses the Ohmic region of operation and while I_D remains constant, its value does not depend on the applied V_{gs} anymore. The system conducts the maximum current value allowed by the transistor, where V_{ds} is theoretically close to 0 V (SCC condition).

The mentioned parameters ($V_{gs(th)}$ and $V_{gs(on)}$) are proportionated by the transistor manufacturer and are characteristic of the MOSFET model employed (IRFZ44N in our experiments) and are reported in Table S2. The transconductance coefficient of the MOSFET was calculated and then was used to determine the relation between V_{gs} , which represents the supplied voltage to the MOSFET, and the I_D demanded to the power generation device. By this, an operating region of the DCELM can be estimated by establishing a V_{gs} range between $V_{gs(th)}$ and $V_{gs(on)}$.

I_D demanded can be divided into a total number of steps for data capture (NS), according to the desired number of experimental points for the characterization. To assure the stabilization of the output current and voltage signals among the transition between the current steps, a control step cycle was incorporated to set a number of repetitions at this condition, which is denominated number of measurements per step (ρ), in order to obtain an average value at the corresponding step condition in data capture.

On the other side, the data acquisition and signal conditioning module is integrated by a coupling circuit between the g terminal and a 12-bit digital—analogue converter (DAC), which can generate voltage steps from 1.22×10^{-3} V up to 1.5 V proportional to 500 mA, which is the maximum current demand of the device and by this generating the signals. It is composed by an ATmega2560 to generate a voltage reference ($ref_{V_{gs}}[\rho]$) through I2C communication with the analogue—digital converter (ADC), in order to measure the current and voltage response of the power generation device ($I_{Load}[\rho]$ and $U_{Load}[\rho]$). By this, the DCELM can obtain the output voltage of the RED unit at a defined current demand

condition, dividing output current range into several steps and measurements per step and operate as a CC mode system.

2.3. The RED Process Characterization

Figure 5 shows a schematic representation of the lab scale RED process. Three working solutions were used: HC and LC solutions as feed waters and ERS. The feed waters flow in a continuous-flow mode through the system, while the ERS flow in a recycle loop between electrode compartments at the endplate and a dark container to isolate it from light.

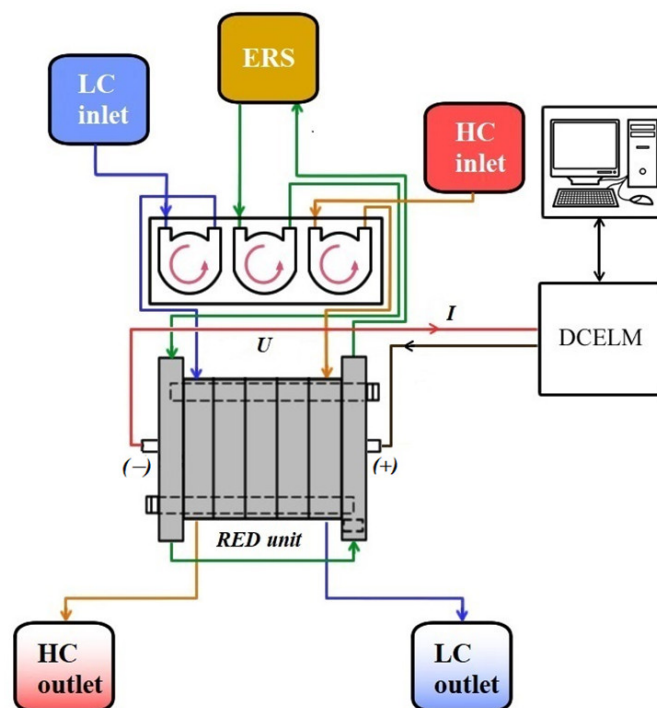


Figure 5. Schematic diagram of lab scale RED process.

All working solutions are fed through one peristaltic pump Masterflex L/S (Cole Parmer, USA) by assembling two pump heads to the same rotor. One of the pump heads has a double channel for HC and LC solutions, so the volumetric flow of each stream is the same, while the other has a single channel for ERS. Figure S5 shows a picture of the lab scale experimental setup of the RED test bench, on which the three main components are indicated: the working solutions system, the RED unit, and the DCELM. The feed parameters are shown in Table 3.

Table 3. Considered feed parameters.

Feed Parameters	RU1
High concentration solution (HC)	0.5133 M
Low concentration solution (LC)	0.0171 M
Electrode rinse solution (ERS)	$[\text{Fe}(\text{CN})_6]^{-4}/[\text{Fe}(\text{CN})_6]^{-3}$ 0.05 M/0.05 M and NaCl 0.25 M as supporting electrolyte
Temperature (T)	298 K
Linear flow velocity (v)	1.0 cm s^{-1} (46 mL min^{-1})

Pure NaCl (Fermont, Mexico. Composition > 99.5%) solutions were used for all the experiments. The concentrations selected represent synthetic river water (0.0171 M) and synthetic seawater (0.5133 M) [32]. All solutions were prepared using deionized water (Fermont, Mexico. Specific Conductance: $1.8 \times 10^{-6} \text{ ohm}^{-1} \text{ cm}^{-1}$). For temperature

control, a hot plate magnetic stirrer C-MAG HS7 (IKA, Königswinter, Germany) and glass thermometers were employed.

The DCELM was connected to the RED unit by a DB9 adaptor with alligator clips. Data capture was performed at a frequency of 0.5 Hz, equivalent to 2 s per measurement. In order to evaluate the differences on data capture setup (DCS) conditions, RED experiments were performed in the Ohmic region of the MOSFET. The resulting current output is divided in a total number of steps for data capture (NS) of 10, 50, and 100 with a number of measurements per step (ρ) of 10 and 20 for each DCS. For all experiments, a temperature of 298 K was used, the pump was calibrated to operate at a linear flow velocity of $1.0 \text{ cm}\cdot\text{s}^{-1}$ and the system was operated for ten minutes at OCV conditions until the voltage signal was completely stable. After that, data capture begins and the output current and voltage raw data are recorded for its processing and plotting. The experiments were repeated three times for every experimental condition described.

2.4. Data Processing of RED Results

Based on the total number of steps for data capture (NS) and the number of measurements per step (ρ) selected on the DCS, the data raw captured were analyzed as follows. An average value of the output current and voltage raw data was calculated for each step condition, according to the ρ selected. For the first step condition, the average values of current and voltage were obtained as is described in Equation (1):

$$M_s = \frac{\sum_{i=1}^{\rho} M_i}{\rho} \quad (1)$$

where M_i and M_s are the raw measurements and the resulting average measurement per step, respectively, (which can be output current or voltage) at the first step condition. Because of the structure of the MATLAB[®] script prepared for this work, for the following steps after first, one measurement less than the ρ selected must be considered. Then, according to the M_s of each step, considering the ρ selected and the adjustment after the first step, the percentage of standard deviation per step ($\%DS$) was calculated for each step as it is showed in Equation (2), and by this the repeatability of the measurements that composed a step was evaluated:

$$\%DS_i = \left(\left(\sqrt{\frac{\sum_{i=1}^{\rho} (M_i - M_s)^2}{\rho - 1}} \right) \div M_s \right) \times 100 \quad (2)$$

To estimate the general uncertainty related to the repeatability of measurements per step inside the operational region of the RED unit, a general percentage of standard deviation per step ($\%GDS$) was considered as an average of individual $\%DS$ values between a selected output current range.

$$\%GDS = \frac{\sum_{i=1}^S (\%DS)_i}{S} \quad (3)$$

where S is the number of steps considered for analysis and its value depends on the DCS selected and the resulting polarization and power curves. The S values are described in Section 3 for every set of experiments. After this, the average general percentage of standard deviation per step ($\%AGDS$) was obtained according to Equation (4), where E is the number of experiments performed at a defined condition, in order to evaluate the average general uncertainty of the obtained output steps for all experiments performed under a certain condition.

$$\%AGDS = \frac{\sum_{i=1}^E (\%GDS)_i}{E} \quad (4)$$

The resulting average measurement per step, obtained by means of Equation (1), represents the obtained output current and voltage values per step and were used to obtain

the corresponding P_d values, using Equations (A10) and (A11) of Appendix A. After this, an average output step (AOS) value was calculated as its own standard deviation for average output step (DAOS) by means of Equations (5) and (6), respectively:

$$AOS = \frac{\sum_{n=1}^E M_n}{E} \quad (5)$$

$$DAOS = \sqrt{\frac{\sum_{n=1}^E (M_n - AOS)^2}{E - 1}} \quad (6)$$

where M_n are the resulting output values per step and it can be referred to I , U , or P_d ; E is the number of experiments performed. The AOS values were used to plot the corresponding polarization and power curves at each DCS tested and the DAOS was used to evaluate the individual uncertainty related to the repeatability of the AOS, which values are expressed in terms of error bars. DAOS value was also obtained in terms of percentage (%DAOS), and a general percentage of standard deviation for average output steps (%GDAOS) was obtained.

$$\%GDAOS = \frac{\sum_{i=1}^S (\%DAOS)_i}{S} \quad (7)$$

where S is the number of steps considered for analysis selected in Equation (3), based on the obtained output current range. This parameter was used to evaluate the general uncertainty related to the repeatability of results in performance curves inside the operational region of the RED unit.

3. Results and Discussion

Evaluation of Data Capture Setup

The output current and voltage raw data obtained using RU1 at the described feed parameters in Table 3, were recorded by the MATLAB[®] interface, and then exported for processing and plotting to evaluate the influence of DCS on accuracy of electrical parameters. Table 4 describes the DCS studied and compared.

Table 4. Data capture setup employed for RED experiments.

Data Capture Setup (DCS)		Steps Considered for Analysis (S)
N ^o Steps (NS)	Number of Measurements per Step (ρ)	
10	10	4
10	20	
50	10	15
50	20	
100	10	30
100	20	

The DCELM was operated only in the Ohmic region of the MOSFET and Figure 6 shows the measurements that conform the steps considered for analysis (S) of one representative experiment at each DCS, between an output current range of approximately 0.007–0.06 A. The raw experimental data are grouped in different colors according to the obtained current and voltage step. For every DCS, two plots are shown: the left side describes current raw data vs. number of measurements while the right side describes voltage raw data vs. number of measurements. As can be seen, the resulting steps are delimited by the ρ selected and one transition measurement between one step to the next is present.

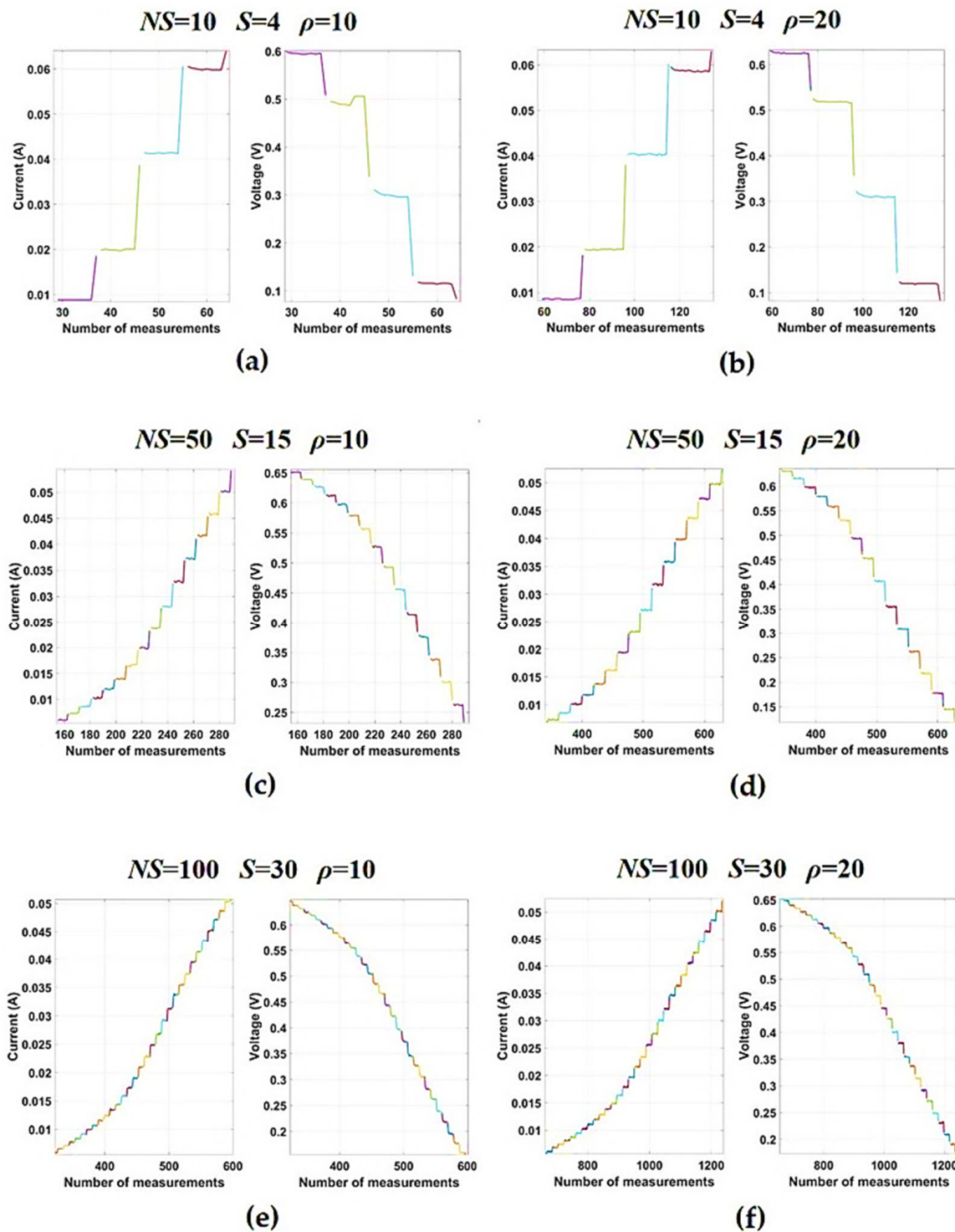


Figure 6. Obtained raw data for current (left side plots) and voltage (right side plots) vs. number of measurements, in a current range from 0.007–0.06 A, at different DCS: (a) $NS = 10$, $\rho = 10$; (b) $NS = 10$, $\rho = 20$; (c) $NS = 50$, $\rho = 10$; (d) $NS = 50$, $\rho = 20$; (e) $NS = 100$, $\rho = 10$ and (f) $NS = 100$, $\rho = 20$. (NS : Total number of steps for data capture; S : steps considered for analysis and ρ : Number of measurements per step). Data are grouped in different colors according to the corresponding current and voltage step.

In order to evaluate the influence of DCS on the repeatability of output current and voltage raw measurements per step, the %DS was calculated for every current and voltage step condition in a range of approximately 0.007–0.06 A for each experiment and then the

%GDS was obtained at this current range for every set of results. Later, the %AGDS of three experiments ($E = 3$) was obtained from the %GDS values and these results are presented in Table 5. According to them, the %AGDS decreases when a ρ of 20 measurements per step is selected compared to a ρ of 10 measurements per step, as well as if a higher number of steps is employed (10, 50, or 100 steps). This trend was attributed to the time it takes to the RED unit to achieve stability on its electromotive force, so as the ρ increases, the uncertainty of obtained output steps will do it too, increasing the precision of results. In the same way, as a higher number of steps are used, the transition from one step to the next one will be shorter, allowing the RED unit achieve a stability condition in a shorter time, enhancing repeatability and by this the precision of the resulting steps.

Table 5. Average general percentage of standard deviation per step (%AGDS) for current and voltage steps, obtained at each DCS.

%AGDS	NS = 10	NS = 10	NS = 50	NS = 50	NS = 100	NS = 100
	$\rho = 10$	$\rho = 20$	$\rho = 10$	$\rho = 20$	$\rho = 10$	$\rho = 20$
Current	13.38	9.97	4.83	3.07	2.20	1.50
Voltage	9.08	5.90	1.88	1.70	1.30	1.01

For visualization and comparison of the electrical parameters at each DCS, the resulting output values per step, obtained by means of Equation (1), were used to determine the AOS with the results of three experiments ($E = 3$) using Equation (5). The calculated AOS were used to construct polarization and power curves at each DCS, as is shown in Figure 7. With the aim of assessing the individual uncertainty related to the repeatability of the AOS, the corresponding DAOS was calculated for every step plotted of each data set (the values of which are represented by error bars in Figure 7), according to Equation (6).

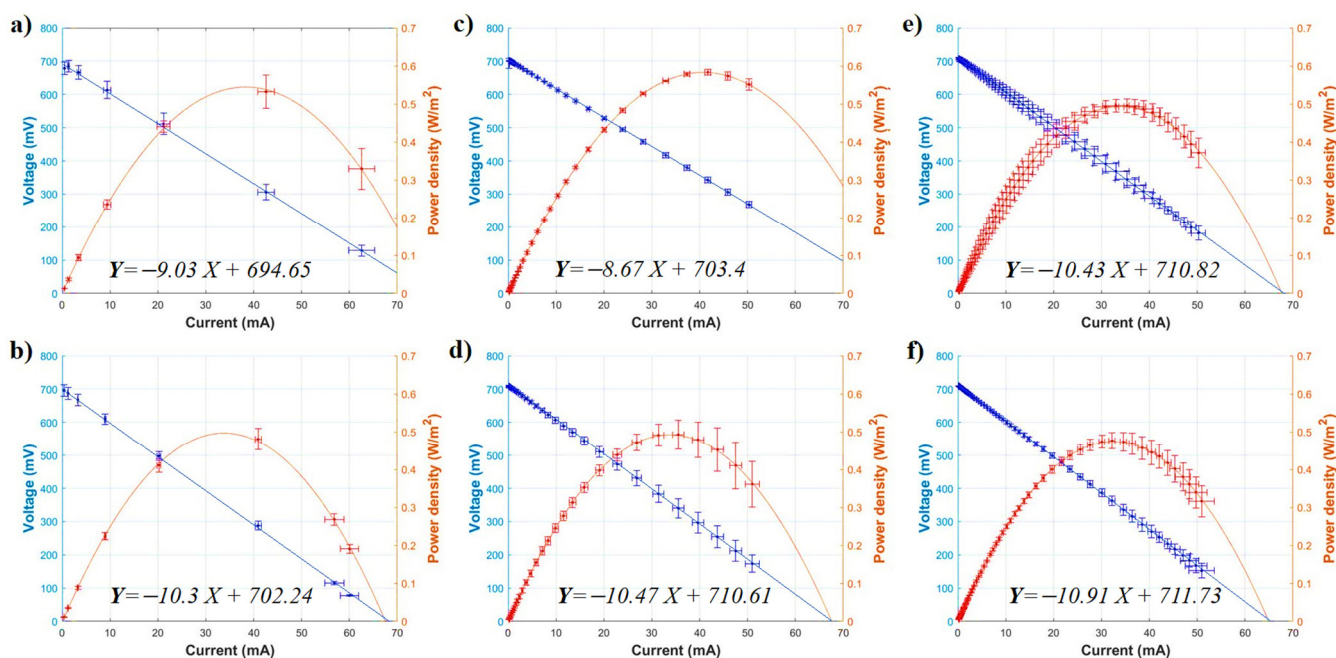


Figure 7. Voltage (mV) vs. current (mA) (blue color, left) and power density (W m^{-2}) vs. current (mA) (red color, right) obtained from the average output steps, at different DCS: (a) NS = 10, $\rho = 10$; (b) NS = 10, $\rho = 20$; (c) NS = 50, $\rho = 10$; (d) NS = 50, $\rho = 20$; (e) NS = 100, $\rho = 10$ and (f) NS = 100, $\rho = 20$.

Linear regression was used to calculate the slope of all polarization curves and by this obtain the internal resistance of RU1 under the described RED process parameters, according to Equation (A7) of the Appendix A. The corresponding linear regression and

resulting values are also indicated. According to these, for all measurements conditions an OCV_{stack} between 694–711 mV was obtained, as well as an R_i between 8.6–10.9 Ω . As for $P_{d max}$, the obtained results were between 0.47–0.58 $W m^{-2}$. The output current range for analysis (approximately 0.007–0.06 A) was selected based on the $P_{d max}$ obtained in the resulting power curves (Figure 7), who was around 40 mA, so our analysis focused on most of the steps before the top of the power curve (which is the maximum power generation zone) and only a few after, since from a technical perspective, it results more convenient to operate the RED unit at lower currents than at higher to generate the same power, because the system is more stable and the deviation values are lower. The %GDAOS for output current, voltage, and power density steps were obtained, at the mentioned output current range, using Equation (7). These values, as the rest of the considered electrical parameters, are indicated in Table 6.

Table 6. Electrical parameters and general percentage of standard deviation for average output steps (%GDAOS) obtained at each DCS.

Electrical Output Parameters	NS = 10	NS = 10	NS = 50	NS = 50	NS = 100	NS = 100
	$\rho = 10$	$\rho = 20$	$\rho = 10$	$\rho = 20$	$\rho = 10$	$\rho = 20$
OCV_{Stack} (mV)	694.65	702.24	703.4	710.61	710.82	711.73
OCV_{Theo} (mV)				838.4		
$P_{d max}$ ($W m^{-2}$)	0.5323	0.4806	0.5813	0.4928	0.4956	0.4766
R_i (Ω)	9.03	10.3	8.67	10.47	10.43	10.91
$\bar{\alpha}$ (%)	82.85	83.75	83.89	84.75	84.78	84.89
%GDAOS—I	5.78	2.17	1.62	4.63	10.46	2.08
%GDAOS—U	7.55	3.49	1.27	5.44	5.18	3.94
%GDAOS— $P_{d max}$	8.38	5.02	1.26	7.10	8.60	4.63

Theoretical open circuit voltage (OCV_{Theo}) was calculated using the Nernst equation and based on its value the apparent permselectivity ($\bar{\alpha}$) was obtained. Both equations can be consulted in Appendix A.

For all cases, the OCV_{Stack} (and consequently $\bar{\alpha}$) increases as a greater NS and ρ are selected, moving towards the calculated OCV_{Theo} and specific permselectivity values provided by the manufacturer (presented in Table S1), firstly because the RED device has twice the time and measurements per step to stabilize the output current and voltage signals, and secondly because it allows the system to have lower changes on the transition between one step to the next, improving the stabilization among these and decreasing the uncertainty of obtained output steps. Moreover, as a greater number of steps the resolution of the resulting polarization and power curves its enhanced, allowing a more refined identification of the operational region and the $P_{d max}$ value. This would be translated in a higher trueness linear regression since it is composed by a greater number of output steps, so the resulting Y interception and slope are more representative of the OCV_{Stack} and R_i values, respectively.

In accordance with the results presented on Figure 7 and Table 6, for polarization and power curves obtained at NS = 100, the operational region has the best resolution, allowing to identify more precisely the maximum power generation zone and the $P_{d max}$ value. When selected ρ is increased at this NS, the uncertainty of resulting electrical parameters decreases notoriously in both %AGDS and %GDAOS values. In this sense, the lowest %AGDS of all DCS studied was obtained using NS = 100 and $\rho = 20$, and in case of AOS, at this DCS the resulting %GDAOS for I, U and $P_{d max}$ were lower than 5%. Hence, by considering the precision of the resulting output current and voltage steps and the uncertainty of AOS, a DCS of NS = 100 and $\rho = 20$ represents the most accurate and reliable approximation of electrical parameters of RU1 using CC mode at the described RED process parameters, among the DCS studied for lab scale RED characterization.

On the other hand, when a DCS of NS = 10 and $\rho = 20$ was used, the obtained $P_{d max}$ value was 0.4806 $W \cdot m^{-2}$, while at NS = 50 and $\rho = 20$ the obtained result was 0.4928 $W \cdot m^{-2}$,

even though the R_i obtained by linear regression was lower at the first DCS mentioned (10.3 Ω and 10.47 Ω , respectively). When the resulting polarization and power curves are compared, in the first case ($NS = 10$, $\rho = 20$) the low NS employed on data capture does not allow to define with more precision the maximum power generation zone, so even when the reported $P_{d\ max}$ represents the highest value among the AOS obtained at this DCS, when the continuous line that corresponds to basic quadratic fitting is observed, this experimental point is located at the right side of the top of power curve, so its value might result in a underestimation of the real $P_{d\ max}$ under the described RED process parameters. In the second case ($NS = 50$ and $\rho = 20$), maximum power generation zone is more well defined and the resulting highest value in power curve is a more representative approximation of $P_{d\ max}$ in RED at those conditions. Nevertheless, as can be seen in error bars of resulting plots at this DCS, the uncertainty of AOS was larger, and values obtained by linear regression would be expected to be less accurate.

Furthermore, the selected number of measurements on every step must be considered given that, as greater ρ selected, the %DS decreases along the operational region of the RED unit, which is traduced in a lower %AGDS for resulting output current and voltage steps and represents higher accuracy on the results used to construct polarization and power curves, the same as the resulting OCV_{Stack} and R_i , consequently. This could be observed when a DCS of $NS = 50$ and $\rho = 10$ was selected, given that although the lowest %GDAOS values for I , U , and $P_{d\ max}$ were obtained, in this scenario the %AGDS for current and voltage steps was higher than by using a larger NS or ρ values. This suggests a poorer stabilization of the output current and voltage raw data, which would cause a higher uncertainty of the obtained steps, producing an overestimation of $P_{d\ max}$. In this sense, when the NS and ρ selected increases, estimated R_i trends to rise and $P_{d\ max}$ to fall, and a lower %AGDS is obtained as is showed in Tables 5 and 6.

The obtained results suggest that data capture conditions have a direct influence on the obtained electrical parameters and its accuracy. Thus, even when the most accurate results, among the studied DCS, were obtained at $NS = 100$ and $\rho = 20$ according to the employed methodology, it is clear that by exploring more DCS the accuracy of results can be improved. In case of apparent permselectivity, despite the fact that this parameter describes in a general form the ability of the membranes to allow the pass to counter-ions and inhibits it for co-ions, assuming that both CEM and AEM have the same value, the obtained $\bar{\alpha}$ at $NS = 100$ and $\rho = 20$ ($\bar{\alpha} = 84.89\%$) was lower than the specific permselectivities values proportioned by the manufacturer (reported in Table S1). In this sense, according to the trend of $\bar{\alpha}$ results in Table 6, if the NS and ρ are increased this could lead to an improvement on stabilization and repeatability of resulting steps, which would be translated into a lower uncertainty and higher accuracy of linear regression values such as OCV_{Stack} . In another aspect, it must also be considered that the employed electrodes in RU1 were not a commercial type, but in-house built. This is relevant since, although commercial Pt/Ti mesh was selected as electrode material, the type of joint employed between the Pt/Ti mesh and the Ti connector, based on a conductive epoxy resin and a conventional epoxy capsulate, might considerably increase the resistance associated with the electrode system, and by this the R_i of the RED unit. This would increase the overpotential of redox reactions, reducing the resulting output voltage on the load and by this reducing the obtained OCV_{Stack} and $\bar{\alpha}$. One way to confirm this last would be to include reference electrodes between the stack and the Pt/Ti mesh electrodes, to determine the OCV condition generated only by the membrane stack without considering the losses in working electrodes, as has been proved in the literature [20,26].

On the other hand, the DC electronic load module (DCELM) developed for this study can be adapted for bench scale or pilot plant scale RED devices, such as others power supply systems, such as Li-ion batteries or fuel cells, taking into account the following requirements: The power module must be scaled according to the current demand range required by the new power supply system, considering that it would need a power dissipation system according to the new demand, which implies adding a forced air or liquid cooling subsystem. Another aspect to be considered is that, in the case of signal acquisition and

conditioning module, the direct measurement on the shut resistance (Figure 4a) should be replaced by an indirect measurement, such as a Hall effect sensor, to isolate the system and protect the circuit against high voltages that may be obtain from the power supply system.

4. Conclusions

The influence of data capture conditions on electrical parameters in reverse electroanalysis (RED) were analyzed employing a DC electronic load module (DCELM), designed and build it for this purpose, and operated in a constant current condition (CC mode). The developed DCELM represents a low-cost alternative to commercial potentiostat/galvanostat and electronic load devices, whose parameters can be controlled to optimize the accuracy of RED characterization. Several data capture setups (DCS) were tested for characterization of lab scale RED process, using an in-house built RED unit prototype (RU1), under the same process parameters. The described methodology in this study evaluates the precision and uncertainty of experimental results, being a quick and reliable option for obtaining a more accurate estimation of the electrical parameters in the RED process on lab scale conditions. In this sense, more DCS might be explored to perform steady state regime tests in benchmark scale or pilot plant scale RED devices. According to results, the accuracy of the resulting current and voltage steps can be enhanced by increasing the total number of steps for data capture (NS), since the repeatability of the measurements within each step increases because the system undergoes fewer changes during the transition from one step condition to the next. Furthermore, as a larger NS is selected, the resolution of the resulting polarization and power curves improves. This enables a clearer identification of the maximum power generation zone in the power curve, as well as more trueness and representative results obtained through linear regression, because the resulting polarization curves are constructed from a greater number of average output steps (AOS). As for the number of measurements per step (ρ), larger values provide the system with additional time for stabilization and a greater number of measurements for step composition, leading to a reduction in the uncertainty of each step, and, by this, increasing its precision and the precision of the AOS consequently. Among the employed DCS in this study, a condition of $NS = 100$ and $\rho = 20$ represented the most accurate setup for data capture at the described experimental conditions using RU1, since the average general percentage of standard deviation per step (%AGDS), of current and voltage steps, were the lowest from all DCS, and the general percentage of standard deviation for average output step (%GDAOS) for output current (I), output voltage (U), and power density ($P_{d\ max}$) were below a 5%, obtaining a high precision and a low uncertainty of the determined electrical parameters inside the operational region of the RED unit. Obtained results in this study suggest that accuracy of electrical parameters can be improved by optimizing the DCS parameters, according to the required specifications and the scale of RED prototypes. Regarding this last, since data capture conditions have a direct influence on results, it may be necessary to define and agree a standardized and feasible methodology of characterization of RED process, which make possible a more representative comparison of results among different research groups.

Supplementary Materials: The following supporting information can be downloaded at: <https://www.mdpi.com/article/10.3390/en16217282/s1>, Figure S1: Equivalent circuit of RED process; Figure S2: RED prototype (RU1) (a) Endplate and stack design, (b) Prototype before assembly; Figure S3: In-house built Pt/Ti mesh electrodes used for RED experiments; Figure S4: DC electronic load module (DCELM); Figure S5: Lab scale experimental setup of the RED test bench. Components of test bench: 1. Low concentration (LC) solution container, 2. High concentration (HC) solution container, 3. Electrode rinse solution (ERS) container, 4. Double head peristaltic pump, 5. RED prototype (RU1), 6. DC electronic load module (DCELM), 7. MATLAB® interface, 8. Hot plate for LC solution and 9. Hot plate for HC solution; Table S1: Properties of IEM used for RED experiments; Table S2: Parameters of the MOSFET IRFZ44N.

Author Contributions: Conceptualization, J.N.H.-P. and M.A.H.-N.; methodology, J.N.H.-P., M.A.H.-N. and J.G.-S.; software, M.A.H.-N.; validation, R.d.G.G.-H. and J.L.R.-R.; formal analysis, J.N.H.-P., M.A.H.-N. and R.d.G.G.-H.; resources, R.d.G.G.-H.; data curation, J.N.H.-P. and M.A.H.-N.;

writing—original draft preparation, J.N.H.-P. and M.A.H.-N.; writing—review and editing, R.d.G.G.-H., J.L.R.-R. and A.O.; visualization, J.N.H.-P. and M.A.H.-N.; supervision, R.d.G.G.-H. and A.O.; project administration, R.d.G.G.-H.; funding acquisition, R.d.G.G.-H. All authors have read and agreed to the published version of the manuscript.

Funding: This research was funded by CONAHCYT-SENER/Sustentabilidad Energética through the Centro Mexicano de Inovación en Energías del Océano (CEMIE-Océano), Grant No. 249795 and by “Proyectos de desarrollo tecnológico o innovación para alumnos del IPN 2021”. Jesus Nahum Hernandez-Perez would like to thank IPN innovation project for students 2021 and the CONACYT for the support provided for project CEMIE Océano 249795. In addition, Rosa de Guadalupe Gonzalez-Huerta would like to thank the support granted by the L’oreal Foundation, UNESCO and the Mexican Academy of Sciences.

Data Availability Statement: Not applicable.

Acknowledgments: The authors want to express their gratitude to “Instituto Politecnico Nacional” (IPN) in Mexico, for the use of their facilities and resources to complete this research work. On the same way, to the Department of Chemical and Biomolecular Engineering of the University of Cantabria for the supervision, supporting and guidance on the preparation of this work. Jesus Nahum Hernandez-Perez would like to thank IPN innovation project for students 2021 and the CONACYT for the support provided for project CEMIE Océano 249795. In addition, Rosa de Guadalupe Gonzalez-Huerta would like to thank the support granted by the L’oreal Foundation, UNESCO and the Mexican Academy of Sciences.

Conflicts of Interest: The authors declare no conflict of interest. The funders had no role in the design of the study; in the collection, analyses, or interpretation of data; in the writing of the manuscript; or in the decision to publish the results.

Nomenclature

Nomenclature	Description	Unit
AOS	Average output step	A, V or $W \cdot m^{-2}$
DAOS	Deviation of average output step	A, V or $W \cdot m^{-2}$
E	Number of experiments performed	-
E_{Cell}	Theoretical electromotive force per cell	V
I	Output current	A
I_D	Theoretical drain current	A
M_i	Raw measurements	A or V
M_n	Resulting output values per step	A, V or $W \cdot m^{-2}$
M_s	Resulting average value at a determined step condition	A or V
N	Number of cells	-
NS	Total number of steps for data capture	-
OCV	Open circuit voltage	V
OCV_{Stack}	Experimental open circuit voltage of the stack	V
OCV_{Theo}	Theoretical open circuit voltage of the stack	V
P_d	Power density	$W \cdot m^{-2}$
$P_{d max}$	Maximum power density	$W \cdot m^{-2}$
R_{Elec}	Electrode system resistance	Ω
R_i	Internal resistance of the RED unit	Ω
R_L	Load resistance	Ω
R_{Stack}	Membrane stack resistance	Ω
S	Number of steps considered for analysis	-
SCC	Short circuit current	A
T	Temperature	K
U	Output voltage	V
v	Linear flow velocity	$cm \cdot s^{-1}$
V_{ds}	Voltage difference between d and s terminals	V
V_{gs}	Voltage difference between g and s terminals	V
$V_{gs(on)}$	Saturation voltage in the g terminal	V
$V_{gs(th)}$	Threshold voltage in the g terminal	V
ΔG_{mix}	Change in Gibbs Free energy upon solutions mixing	kJ

$\bar{\alpha}$	Apparent permselectivity	%
δ	Intermembrane distance	μm
ρ	Number of measurements per step	-
%AGDS	Average general percentage of standard deviation per step	%
%DAOS	Percentage of deviation for average output step	%
%DS	Percentage of standard deviation per step	%
%GDAOS	General percentage of standard deviation for average output step	%
%GDS	General percentage of standard deviation per step	%

Abbreviations

Abbreviations	Description
ABS	Acrylonitrile—Butadiene—Styrene
ADC	Analogical—digital converter
AEM	Anion Exchange Membrane
CC—mode	Constant current condition
CP—mode	Constant power condition
CR—mode	Constant resistance condition
CV—mode	Constant voltage condition
CEM	Cation Exchange Membrane
d	Drain terminal
DAC	Digital—analogical converter
DCELM	DC-Electronic Load Module
DCS	Data Capture Setup
EMF	Electromotive Force
ERS	Electrode Rinse Solution
g	Gate terminal
HC	High Concentration
IEM	Ion Exchange Membrane
I–V mode	Changing current condition
LC	Low Concentration
MOSFET	Metal-Oxide-Semiconductor Field-Effect Transistor
PES	Polyether Sulphone
Pt/Ti mesh	Titanium mesh with platinum coating
RED	Reverse Electrodialysis
RU1	RED Unit 1
s	Source terminal
SGE	Salinity Gradient Energy

Appendix A

The Nernst Equation (A1) describes the electromotive force (EMF) available by each IEM according to the salinity gradient value [10,11,33].

$$E_{CEM} = \alpha_{CEM} \cdot \frac{R \cdot T}{z \cdot F} \cdot \ln \frac{a_{HC_{Na^+}}}{a_{LC_{Na^+}}} = \alpha_{CEM} \cdot \frac{R \cdot T}{z_{Na^+} \cdot F} \cdot \ln \frac{\gamma_{HC_{Na^+}} C_{HC_{Na^+}}}{\gamma_{LC_{Na^+}} C_{LC_{Na^+}}} \quad (A1)$$

E_{CEM} is the EMF generated across the CEM, α_{CEM} is the membrane permselectivity, z the valence of the ionic specie considered ($z = 1$ for Na^+ and Cl^-), R the universal thermodynamic constant ($8.314 \text{ J} \cdot \text{mol}^{-1} \text{ K}^{-1}$), T the temperature in K, F the Faraday constant ($96485 \text{ C} \cdot \text{mol}^{-1}$), and $a_{HC_{Na^+}}$ and $a_{LC_{Na^+}}$ are the activities of Na^+ on the HC and LC solutions, respectively. This last values can be obtained as the product of activity coefficients ($\gamma_{HC_{Na^+}}$, $\gamma_{LC_{Na^+}}$), which value is equal to 1 for ideal solutions, and the concentration of sodium ion on HC and LC solutions ($C_{HC_{Na^+}}$, $C_{LC_{Na^+}}$) in $\text{mol} \cdot \text{m}^{-3}$ [10,11,33]. The Nernst equation can also be expressed in terms of Cl^- for E_{AEM} , the addition of both E_{CEM} and E_{AEM} give as result the cell potential ($E_{CEM} + E_{AEM} = E_{Cell}$) [5,10,11]. The theoretical electrical

potential of the RED unit at the open circuit voltage condition (OCV_{Theo}) can be obtained as by E_{Cell} times the number of cells (N):

$$OCV_{Theo} = N \cdot E_{Cell} \quad (A2)$$

The amount of energy that can be obtained on the RED unit its limited by the available EMF and its internal resistance (R_i). In principle, R_i its conformed by the Ohmic (R_{Ohm}) and non-Ohmic ($R_{non-Ohm}$) components of the RED stack resistance (R_{Stack}) and the electrode system resistance (R_{Elec}). All these parameters are expressed in Ohms:

$$R_i = R_{Stack} + R_{Elec} = N \cdot R_{Ohm} + R_{non-Ohm} + R_{Elec} \quad (A3)$$

The non-Ohmic component of R_i is associated with diffusional boundary layer (DBL) effects and concentration changes across the intermembrane space. On the other hand, the Ohmic components (Equation (A4)) are referred to intrinsically resistance of CEM and AEM (R_{CEM} and R_{AEM}) and the resistance of the flow channels (R_{HCC} and R_{LCC}) in $\Omega \cdot \text{cm}^2$, the term A_{mem} refers to effective area of membrane expressed in cm^2 [5,11,18].

$$R_{Ohm} = \frac{1}{A_{mem}} \cdot [R_{AEM} + R_{CEM} + R_{HCC} + R_{LCC}] \quad (A4)$$

The resistance of the flow channels can be obtained using Equations (A5) and (A6), where δ is the intermembrane space (in cm), C_{HC} and C_{LC} are the molar concentrations of the high concentration and low concentration solutions ($\text{mol} \cdot \text{cm}^{-3}$), σ is the molar conductivity of the species in solution ($\text{S} \cdot \text{cm}^{-1} \text{mol}^{-1}$), and ε is the obstruction factor, a coefficient that increases the resistance in consideration of the negative effects of the spacer to ion transfer [33,34]. From the literature, σ value is $0.08798 \text{ S} \cdot \text{cm}^{-1} \text{mol}^{-1}$ [34].

$$R_{HCC} = \varepsilon \frac{\delta}{\sigma \cdot C_{HC}} \quad (A5)$$

$$R_{LCC} = \varepsilon \frac{\delta}{\sigma \cdot C_{LC}} \quad (A6)$$

When an external load (R_L) is connected to the RED unit, the voltage output (U) in Volts can be calculated as the open circuit voltage condition (OCV_{Theo}), less voltage drop across the internal resistance of the RED unit:

$$U = OCV_{Theo} - I \cdot R_i \quad (A7)$$

where I is the electrical current (in Amperes) generated by the RED unit. By the other side, U can also be calculated from the voltage drop on the external load (R_L):

$$U = I \cdot R_L \quad (A8)$$

Since Equations (A7) and (A8) are equivalent, we can resolve the I term and by this obtain the theoretical current value at different values of external load. By this the theoretical value of I can be obtained [10,11,33]:

$$I = \frac{OCV_{Theo}}{R_i + R_L} \quad (A9)$$

The gross power (P_g) obtained over R_L can be calculated from the product of current and voltage output, according to Equation (A10) [33]:

$$P_g = I \cdot U \quad (A10)$$

P_g can be normalized by dividing its value by the total active area of a cell in the stack, obtaining the power density (P_d). Here, A_{mem} is the membrane active area per cell and N is the number of cells [5,11,18]:

$$P_d = \frac{P_g}{N \cdot A_{mem}} \quad (A11)$$

Linear flow velocity (v) is defined as the fluid speed inside the flow compartments formed in the intermembrane space, as is expressed in $\text{m} \cdot \text{s}^{-1}$ according to Equation (A12) [11]:

$$v_i = \frac{\phi_i}{\varepsilon \cdot N \cdot W \cdot \delta} \quad (A12)$$

where ϕ_i is volumetric flow of HC or LC feed stream in m^3 , ε is the spacer porosity, N is the number of cells, W is the wide of active area on membrane in m, and δ is the intermembrane space in m. Based on stack dimensions and number of cells, it is possible to define an operative v and estimate the volumetric flow required for HC and LC solutions, so Equation (A13) can be reordered as:

$$\phi_{HC} = \phi_{LC} = v \cdot \varepsilon \cdot N \cdot W \cdot \delta \quad (A13)$$

The apparent permselectivity ($\bar{\alpha}$) is a parameter that describes in a general form the ability of the membranes to allow the pass to counter-ions and inhibits it for co-ions (i.e., for CEM Na^+ is the counter-ion while Cl^- is a co-ion) [5,20]. The $\bar{\alpha}$ value can be calculated as in Equation (A14), where OCV_{stack} represents the experimental OCV value.

$$\bar{\alpha} = \frac{\text{OCV}_{stack}}{\text{OCV}_{Theo}} \times 100 \quad (A14)$$

References

- Osorio, A.F.; Arias-Gaviria, J.; Devis-Morales, A.; Acevedo, D.; Velasquez, H.I.; Arango-Aramburo, S. Beyond electricity: The potential of ocean thermal energy and ocean technology ecoparks in small tropical islands. *Energy Policy* **2016**, *98*, 713–724. [CrossRef]
- Sims, R.E.H. Renewable energy: A response to climate change. *Sol. Energy* **2004**, *76*, 9–17. [CrossRef]
- Pawlowski, S.; Crespo, J.; Velizarov, S. Sustainable power generation from salinity gradient energy by reverse electrodialysis. In *Electro-Kinetics across Disciplines and Continents: New Strategies for Sustainable Development*; Springer International Publishing: New York, NY, USA, 2015; pp. 57–80. [CrossRef]
- Post, J.W.; Veerman, J.; Hamelers, H.V.M.; Euverink, G.J.W.; Metz, S.J.; Nijmeijer, K.; Buisman, C.J.N. Salinity-gradient power: Evaluation of pressure-retarded osmosis and reverse electrodialysis. *J. Membr. Sci.* **2007**, *288*, 218–230. [CrossRef]
- Tufa, R.A.; Pawlowski, S.; Veerman, J.; Bouzek, K.; Fontananova, E.; di Profio, G.; Velizarov, S.; Crespo, J.G.; Nijmeijer, K.; Curcio, E. Progress and prospects in reverse electrodialysis for salinity gradient energy conversion and storage. *Appl. Energy* **2018**, *225*, 290–331. [CrossRef]
- Reyes-Mendoza, O.; Alvarez-Silva, O.; Chiappa-Carrara, X.; Enriquez, C. Variability of the thermohaline structure of a coastal hyper-saline lagoon and the implications for salinity gradient energy harvesting. *Sustain. Energy Technol. Assess.* **2020**, *38*, 100645. [CrossRef]
- Yasukawa, M.; Mehdizadeh, S.; Sakurada, T.; Abo, T.; Kuno, M.; Higa, M. Power generation performance of a bench-scale reverse electrodialysis stack using wastewater discharged from sewage treatment and seawater reverse osmosis. *Desalination* **2020**, *491*, 114449. [CrossRef]
- Gómez-Coma, L.; Abarca, J.A.; Fallanza, M.; Ortiz, A.; Ibáñez, R.; Ortiz, I. Optimum recovery of saline gradient power using reversal electrodialysis: Influence of the stack components. *J. Water Process Eng.* **2022**, *48*, 102816. [CrossRef]
- Micale, G.; Cipollina, A.; Tamburini, A. Salinity gradient energy. In *Sustainable Energy from Salinity Gradients*; Elsevier: Amsterdam, The Netherlands, 2016; pp. 1–17. [CrossRef]
- Ortiz-Imedio, R.; Gomez-Coma, L.; Fallanza, M.; Ortiz, A.; Ibáñez, R.; Ortiz, I. Comparative performance of Salinity Gradient Power-Reverse Electrodialysis under different operating conditions. *Desalination* **2019**, *457*, 8–21. [CrossRef]
- Veerman, J.; Vermaas, D.A. Reverse electrodialysis. In *Sustainable Energy from Salinity Gradients*; Elsevier: Amsterdam, The Netherlands, 2016; pp. 77–133. [CrossRef]
- Cahe, S.; Kim, H.; Hong, J.G.; Jang, J.; Higa, M.; Pishnamazi, M.; Choi, J.Y.; Walgama, R.C.; Bae, C.; Kim, I.S.; et al. Clean power generation from salinity gradient using reverse electrodialysis technologies: Recent advances, bottlenecks, and future direction. *Chem. Eng. J.* **2023**, *452*, 139482. [CrossRef]
- Veerman, J.; Saakes, M.; Metz, S.J.; Harmsen, G.J. Reverse electrodialysis: Evaluation of suitable electrode systems. *J. Appl. Electrochem.* **2010**, *40*, 1461–1474. [CrossRef]

14. Jang, J.; Kang, Y.; Han, J.H.; Jang, K.; Kim, C.M.; Kim, I.S. Developments and future prospects of reverse electrodi-alysis for sa-linity gradient power generation: Influence of ion exchange membranes and electrodes. *Desalination* **2020**, *491*, 114540. [[CrossRef](#)]
15. Scialdone, O.; Guarisco, C.; Grispo, S.; Angelo, A.D.; Galia, A. Investigation of electrode material—Redox couple systems for reverse electrodi-alysis processes. Part I: Iron redox couples. *J. Electroanal. Chem.* **2012**, *681*, 66–75. [[CrossRef](#)]
16. Scialdone, O.; Albanese, A.; D’Angelo, A.; Galia, A.; Guarisco, C. Investigation of electrode material—Redox couple systems for reverse electrodi-alysis processes. Part II: Experiments in a stack with 10–50 cell pairs. *J. Electroanal. Chem.* **2013**, *704*, 1–9. [[CrossRef](#)]
17. Lee, S.Y.; Jeong, Y.J.; Chae, S.R.; Yeon, K.H.; Lee, Y.; Kim, C.S.; Jeong, N.J.; Park, J.S. Porous carbon-coated graphite electrodes for energy production from salinity gradient using reverse electrodi-alysis. *J. Phys. Chem. Solids* **2016**, *91*, 34–40. [[CrossRef](#)]
18. Mei, Y.; Tang, C.Y. Recent developments and future perspectives of reverse electrodi-alysis technology: A review. *Desalination* **2018**, *425*, 156–174. [[CrossRef](#)]
19. Ortiz-Martínez, V.M.; Gómez-Coma, L.; Tristán, C.; Pérez, G.; Fallanza, M.; Ortiz, A.; Ibañez, R. A comprehensive study on the effects of operation variables on reverse electrodi-alysis performance. *Desalination* **2020**, *482*, 114389. [[CrossRef](#)]
20. Długołęcki, P.; Gambier, A.; Nijmeijer, K.; Wessling, M. Practical potential of reverse electrodi-alysis as process for sustainable energy generation. *Environ. Sci. Technol.* **2009**, *43*, 6888–6894. [[CrossRef](#)]
21. Roldan-Carvajal, M.; Vallejo-Castaño, S.; Álvarez-Silva, O.; Bernal-García, S.; Arango-Aramburo, S.; Sánchez-Sáenz, C.I.; Osorio, A.F. Salinity gradient power by reverse electrodi-alysis: A multidisciplinary assessment in the Colombian context. *Desalination* **2021**, *503*, 114933. [[CrossRef](#)]
22. Sandoval-Sánchez, E.; de la Cruz-Barragán, Z.; Miranda-Hernández, M.; Mendoza, E. Effect of Gaskets Geometry on the Performance of a Reverse Electrodi-alysis Cell. *Energies* **2022**, *15*, 3361. [[CrossRef](#)]
23. Tedesco, M.; Scalici, C.; Vaccari, D.; Cipollina, A.; Tamburini, A.; Micale, G. Performance of the first reverse electrodi-alysis pilot plant for power production from saline waters and concentrated brines. *J. Membr. Sci.* **2016**, *500*, 33–45. [[CrossRef](#)]
24. Avci, A.H.; Rijnaarts, T.; Fontanova, E.; Di Profio, G.; Vankelecom, I.F.V.; De Vos, W.M.; Cursio, E. Sulfonated polyethersulfone based cation exchange membranes for reverse electrodi-alysis under high salinity gradients. *J. Membr. Sci.* **2020**, *595*, 117585. [[CrossRef](#)]
25. Mehdizadeh, S.; Yasukawa, M.; Kuno, M.; Kawabata, Y.; Higa, M. Evaluation of energy harvesting from discharged solutions in a salt production plant by reverse electrodi-alysis (RED). *Desalination* **2019**, *467*, 95–102. [[CrossRef](#)]
26. Veerman, J.; Saakes, M.; Metz, S.J.; Harmsen, G.J. Reverse electrodi-alysis: Performance of a stack with 50 cells on the mixing of sea and river water. *J. Membr. Sci.* **2009**, *327*, 136–144. [[CrossRef](#)]
27. Benneker, A.M.; Rijnaarts, T.; Lammertink, R.G.H.; Wood, J.A. Effect of temperature gradients in (reverse) electrodi-alysis in the Ohmic regime. *J. Membr. Sci.* **2018**, *548*, 421–428. [[CrossRef](#)]
28. Güler, E.; Elizen, R.; Vermaas, D.A.; Saakes, M.; Nijmeijer, K. Performance-determining membrane properties in reverse electrodi-alysis. *J. Membr. Sci.* **2013**, *446*, 266–276. [[CrossRef](#)]
29. Gómez-Coma, L.; Ortiz-Martínez, V.M.; Carmona, J.; Palacio, L.; Prádanos, P.; Fallanza, M.; Ortiz, A.; Ibañez, R.; Ortiz, I. Modeling the influence of divalent ions on membrane resistance and electric power in reverse electrodi-alysis. *J. Membr. Sci.* **2019**, *592*, 117385. [[CrossRef](#)]
30. Electronic Load Fundamentals. Available online: <https://www.keysight.com/us/en/assets/7018-06481/white-papers/5992-3625.pdf> (accessed on 18 October 2023).
31. Hong, J.G.; Chen, Y. Nanocomposite reverse electrodi-alysis (RED) ion-exchange membranes for salinity gradient power generation. *J. Membr. Sci.* **2014**, *460*, 139–147. [[CrossRef](#)]
32. Marin-Coria, E.; Silva, R.; Enriquez, C.; Martínez, M.L.; Mendoza, E. Environmental assessment of the impacts and benefits of a salinity gradient energy pilot plant. *Energies* **2021**, *14*, 3252. [[CrossRef](#)]
33. Veerman, J.; Saakes, M.; Metz, S.J.; Harmsen, G.J. Reverse electrodi-alysis: A validated process model for design and optimization. *Chem. Eng. J.* **2011**, *166*, 256–268. [[CrossRef](#)]
34. Yip, N.Y.; Vermaas, D.A.; Nijmeijer, K.; Elimelech, M. Thermodynamic, energy efficiency, and power density analysis of reverse electrodi-alysis power generation with natural salinity gradients. *Environ. Sci. Technol.* **2014**, *48*, 4925–4936. [[CrossRef](#)]

Disclaimer/Publisher’s Note: The statements, opinions and data contained in all publications are solely those of the individual author(s) and contributor(s) and not of MDPI and/or the editor(s). MDPI and/or the editor(s) disclaim responsibility for any injury to people or property resulting from any ideas, methods, instructions or products referred to in the content.